Integration of airborne and ground observations of nitryl chloride in the Seoul metropolitan area and the implications on regional oxidation capacity during KORUS-AQ 2016

Daun Jeong, Roger Seco, Dasa Gu, Youngro Lee, Benjamin A. Nault, Christoph Knote, Tom Mcgee, John T. Sullivan, Jose L. Jimenez, Pedro Campuzano-Jost, Donald R. Blake, Dianne Sanchez, Alex B. Guenther, David Tanner, L. Gregory Huey, Russell Long, Bruce E. Anderson, Samuel R. Hall, Kirk Ullmann, Hye-jung Shin, Scott C. Herndon, Youngjae Lee, Danbi Kim, Joonyoung Ahn, Saewung Kim

Angaben zur Veröffentlichung / Publication details:

Jeong, Daun, Roger Seco, Dasa Gu, Youngro Lee, Benjamin A. Nault, Christoph Knote, Tom Mcgee, et al. 2019. "Integration of airborne and ground observations of nitryl chloride in the Seoul metropolitan area and the implications on regional oxidation capacity during KORUS-AQ 2016." *Atmospheric Chemistry and Physics* 19 (19): 12779–95. https://doi.org/10.5194/acp-19-12779-2019.

Supplement of Atmos. Chem. Phys., 19, 12779–12795, 2019
https://doi.org/10.5194/acp-19-12779-2019-supplement

Atmospheric Chemistry and Physics
Open Access
EGU

Supplement of

Integration of airborne and ground observations of nitryl chloride in the Seoul metropolitan area and the implications on regional oxidation capacity during KORUS-AQ 2016

Daun Jeong et al.

Correspondence to: Saewung Kim (saewung.kim@uci.edu)

S1. Configuration of the chemical ionization mass spectrometer during the KORUS-AQ campaign

During the KORUS-AQ 2016 field campaign a chemical ionization mass spectrometer (CIMS) was deployed to measure Cl_2 and $ClNO_2$. These systems were deployed at the Taehwa Research Forest (TRF), Olympic Park (OP), and on-board the NASA DC-8. The configuration of the inlet at the two ground sites is shown in Figure S1. The CIMS on the DC-8 had a similar configuration but without the heating inlet.

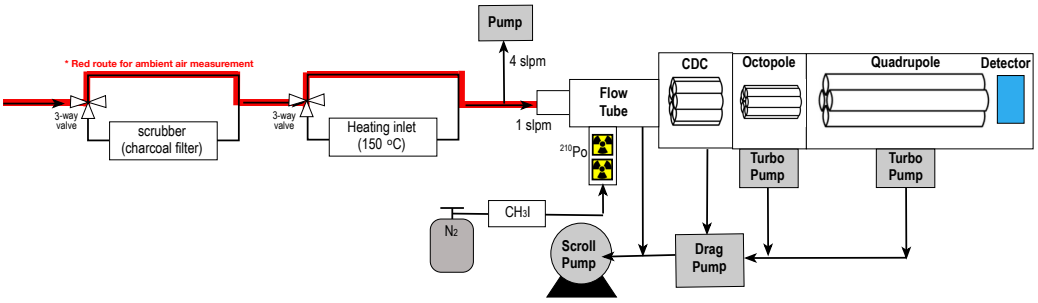

Figure S1. Configuration of the CIMS inlet at the TRF and OP during KORUS-AQ 2016.

S2. Description of the Extended Aerosol Inorganics Model

To calculate aerosol liquid water mass concentration and the acidity (pH) of the aerosol, the Extended Aerosol Inorganic Model (E-AIM) was used (Clegg et al., 1998; Friese and Ebel, 2010). Prior studies have shown that either E-AIM and the ISORROPIA-II model can be used to calculate aerosol liquid water concentration and pH, as both thermodynamic models predict similar values (Hennigan et al., 2015; Song et al., 2018). The E-AIM model was run in the reverse mode. This has been found to be the optimal mode (Hennigan et al., 2015; Song et al., 2018), as it minimizes the errors in the measurements, leading more stable results that better represents the observations. Reverse mode means that total nitrate (aerosol plus gas-phase), sulfate, ammonium, relative humidity, and temperature were the inputs of the model. Gas-phase HNO_3 was measured by California Institute of Technology chemical ionization mass spectrometer (CIT-CIMS) (Crounse et al., 2006), and the aerosol-phase nitrate, sulfate, and ammonium were measured by the University of Colorado AMS (Nault et al., 2018). Total NH_x was not an input, as there was not a gas-phase measurement of NH_3. Guo et al. (2016) showed that ISORROPIA was still able to properly partition total nitrate between the gas- and particle-phase without NH_3 as an input when the model was ran iteratively to estimate NH_3. The E-AIM model was run similarly here, and it took approximately 20 iterative runs for convergence on the NH_3 concentration that explained the observed partitioning of nitrate between gas- and particle-phase. To validate E-AIM modeled predictions, the modeled predicted vs observed partitioning of nitrate between gas- and particle-phase were compared (Figure S2). Since the partitioning of nitrate between gas- and particle-phase is a function of the amount of water, temperature, and pH of the aerosol (Guo et al., 2016, 2017), a high correlation and a slope near unity indicates that E-AIM is closely representing the pH and liquid water concentrations for sub-micron aerosol. The slopes for HNO_3 and NO_3^- are 1.07 and 0.89, respectively, and the R^2 for HNO_3 and NO_3^- are 0.96 and 0.99, respectively; therefore, E-AIM predicted the observed nitrate partitioning between gas- and particle-phase, providing confidence in the pH and aerosol liquid water concentration.

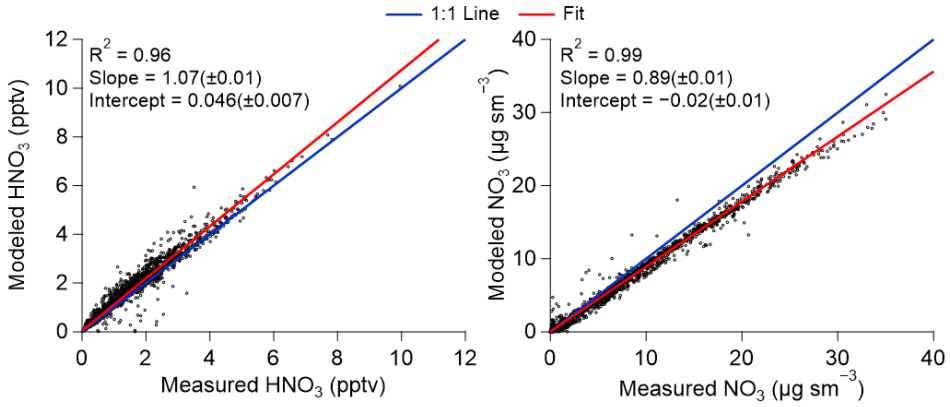

Figure S2. (Left) Comparison of E-AIM modeled and measured (CIT-CIMS) gas-phase HNO_3. (Right) Comparison of E-AIM modeled and measured (CU AMS) particle-phase NO_3^-

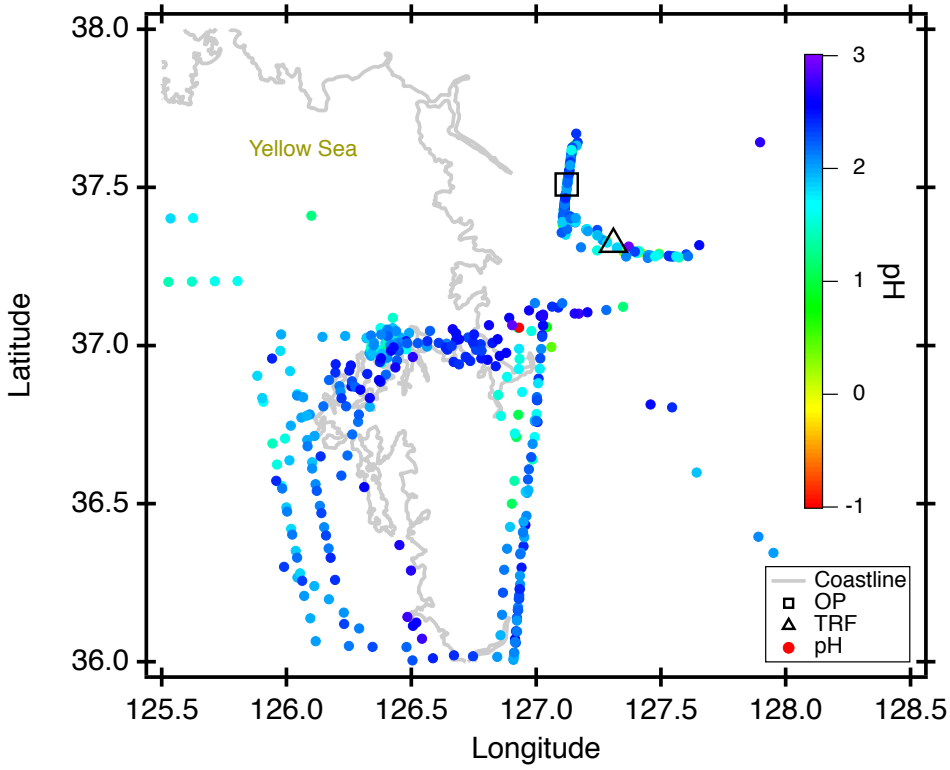

Figure S3. Aerosol pH calculated with E-AIM constrained with airborne measurements.

S3. Description on the setup of the box model

The Framework for 0-D Atmospheric Modeling (F0AM v3.1) was used for box model simulations in this study. For heterogeneous reactions of gas-phase N_2O_5 (i.e., $N_2O_5{}_{(g)}$ + $Cl^-{}_{(aq)} \rightarrow ClNO_2{}_{(g)}$), $ClONO_2$ (i.e., $ClONO_2{}_{(g)}$ + $Cl^-{}_{(aq)}$ + $H^+{}_{(aq)}$ $\rightarrow Cl_2{}_{(g)}$ + HNO_3), and HOCl (i.e., $HOCl_{(g)}$ + $Cl^-{}_{(aq)}$ + $H^+{}_{(aq)} \rightarrow Cl_2{}_{(g)}$ + H_2O), a simple first-order reaction was assumed by accounting for γ, ϕ, molecular speed of the gases, and surface area of aerosols. Hygroscopic growth factor was not considered in the model. γ_{N2O5} was calculated from the Bertram and Thornton (2009) study using measured inorganic aerosol composition, temperature, and relative humidity and water content derived from the thermodynamic model Extended Aerosol Inorganics Model (E-AIMS, (Clegg et al., 1998; Friese and Ebel, 2010)). The average and median γ_{N2O5} values during the whole campaign were both 0.017. This is in the lower range of what has been derived from previous field observations in Asia that ranges from a campaign average of 0.004 to 0.072 (Yun et al., 2018; Brown et al., 2016; Tham et al., 2016; Wang et al., 2017a, c, b). γ values of $ClONO_2$ and HOCl were set to 0.06 (Deiber et al., 2004; Hanson et al., 1994; Hanson and Ravishankara, 1994). The yields (ϕ) of the three heterogeneous reactions were assumed to be 1, therefore the steady state simulations would be an upper-limit of Cl_2 or $ClNO_2$ production. Since we did not have any aerosol size distribution data collected at the ground sites, aerosol surface area was taken from airborne measurements. An averaged value was used from data retrieved below 1 km over the SMA. The airborne data did not show a significant vertical dependence within the daytime boundary layer. Based on this, an average of 78 $\pm 41 \mu m^2$ cm^{-3} were estimated for particle sizes between 10 nm and 5 μm. Impact of measured $ClNO_2$ on O_3 production (Figure 10) was explored by constraining the box model with diurnal variation of observations throughout each step. Constraining the model with the diurnal variation of measured $ClNO_2$, allowed the box model to capture its trend throughout the course of the day. Since our purpose of the simulations were to explore the possible impact of $ClNO_2$ on O_3 production, NO_2 and O_3 were only constrained initially at the first step with observations and then calculated based on the chemistry embedded in the model. More specifically, the initial concentration of each following step was taken from the value in the previous step. The results were compared to the base scenario, in which $ClNO_2$ was not constrained. Net O_3 production rate was calculated in the box model as below, where f is the stoichiometric coefficient of O_3 and k is the rate constant corresponding to each reaction i. More details can be found in the supplements of Wolfe et al. (2016) :

$$d[O_3]/dt = O_3 production rate - O_3 loss rate = \sum_{i=1}^{\sharp of reactions} f_i \times (product of reactions)_i \times k_i \quad (1)$$

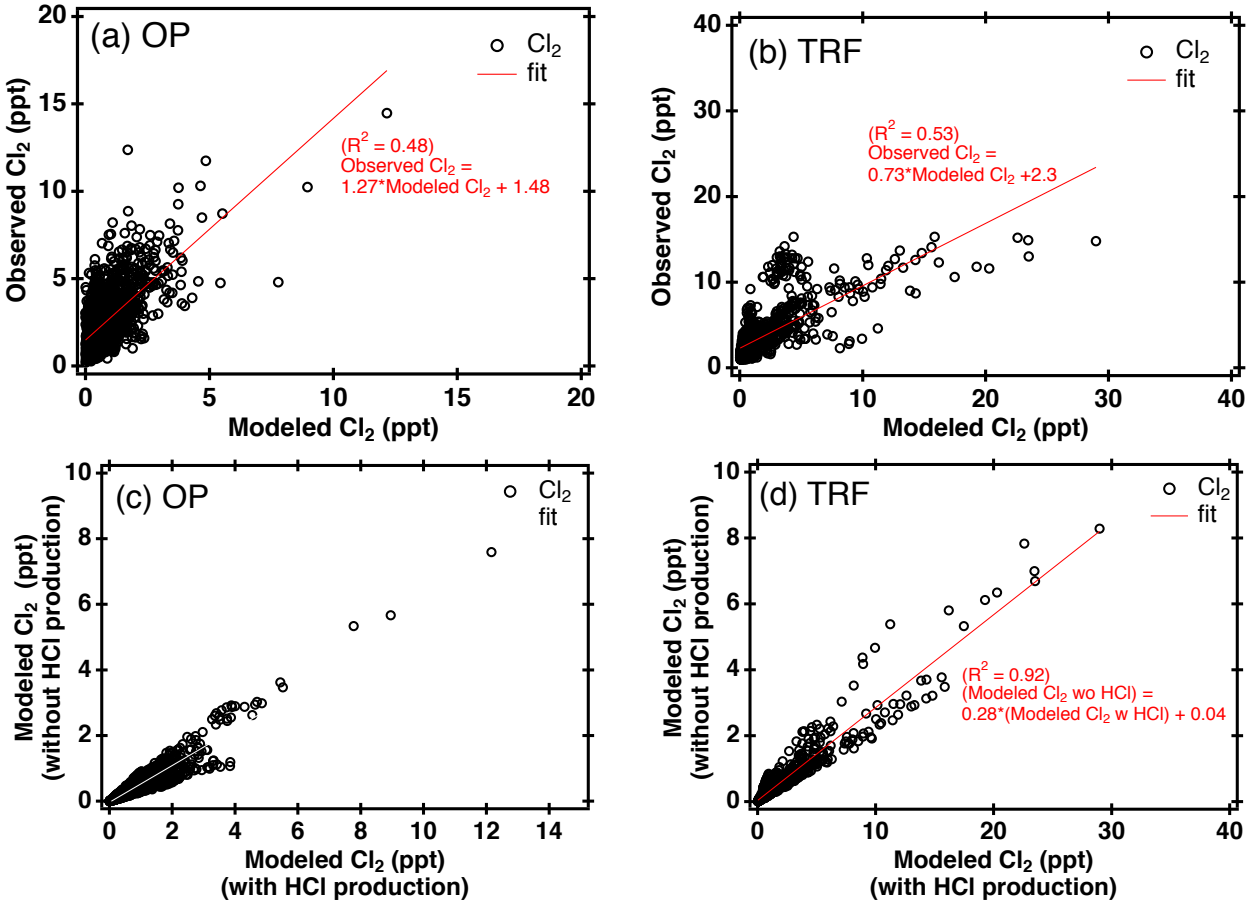

Figure S4. Correlation between measured Cl_2 and modeled Cl_2 at (a) OP and (b) TRF. Sensitivity tests of HCl were carried out (c and d) by switching off HCl production from chlorine radicals reacting with VOCs.

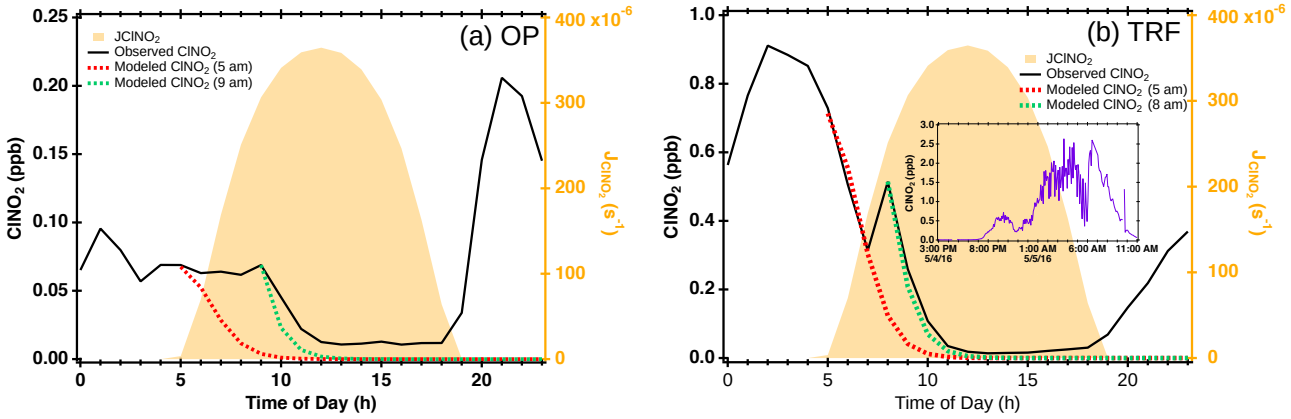

Figure S5. Diurnal variation of measured $ClNO_2$ (black line) and simulated $ClNO_2$ from photolytic loss (dashed line). For the red and green dashed lines, the model was constrained with measured $ClNO_2$ at sunrise and at the time when $ClNO_2$ started decreasing, respectively. J_{ClNO2} used for the photolysis was scaled with airborne measurements. The insert in (b) is the $ClNO_2$ measured on May 5th.

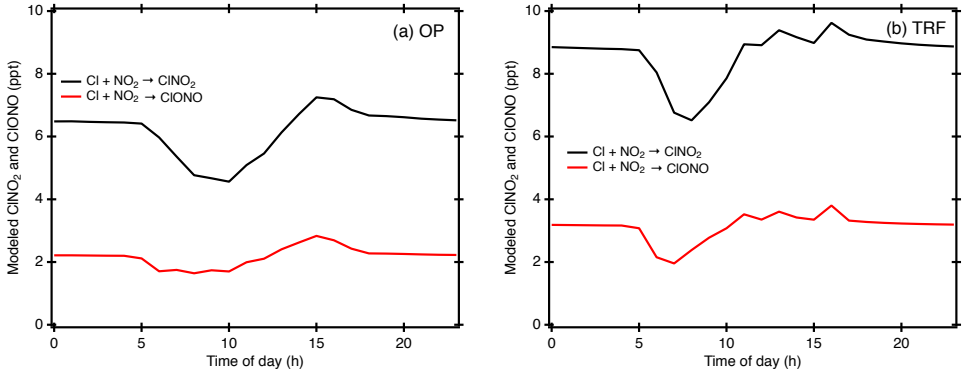

Figure S6. Simulated $ClNO_2$ and ClONO produced from gas phase reaction of Cl· + NO_2 (i.e., $Cl\cdot_{(g)}$ + $NO_{2(g)}$ + M $\rightarrow$ $ClNO_{2(g)}$ + M, k = 3.6×10^{-12}; $Cl\cdot_{(g)}$ + $NO_{2(g)}$ + M $\rightarrow$ $ClONO_{(g)}$ + M, k= 1.63×10^{-12}, (Burkholder et al., 2015)) The model was constrained with Cl_2 and NO_2 observations with J values from the aircraft.

S4. Additional figures of observations during the KORUS-AQ campaign.

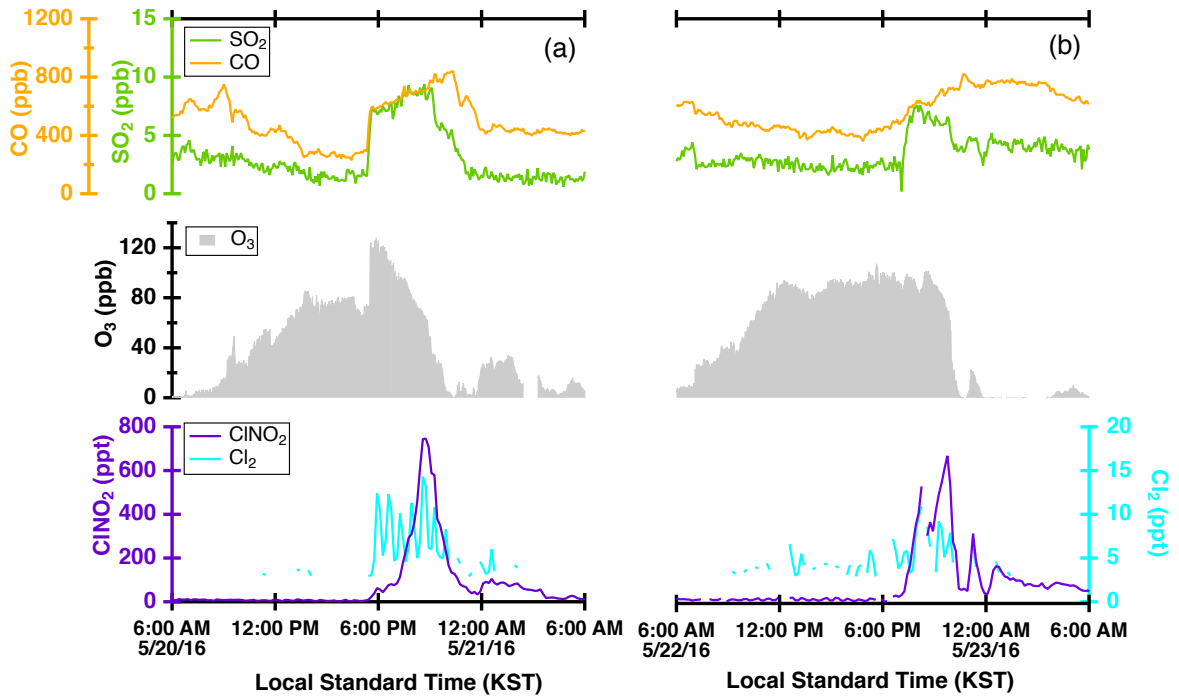

Figure S7. Trace gas measurements at the OP site on May 20th and 22nd.

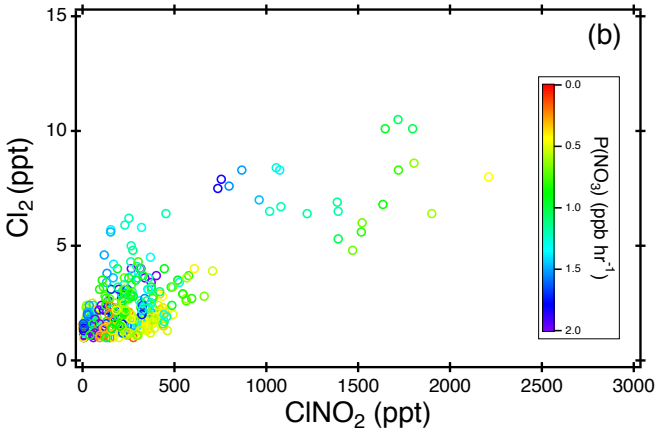

Figure S8. Correlation between Cl_2 and $ClNO_2$ measured at 7:00 - 9:00 am local time. Each data point is a 5 min averaged value and is color coded with the calculated production rate of the nitrate radical.

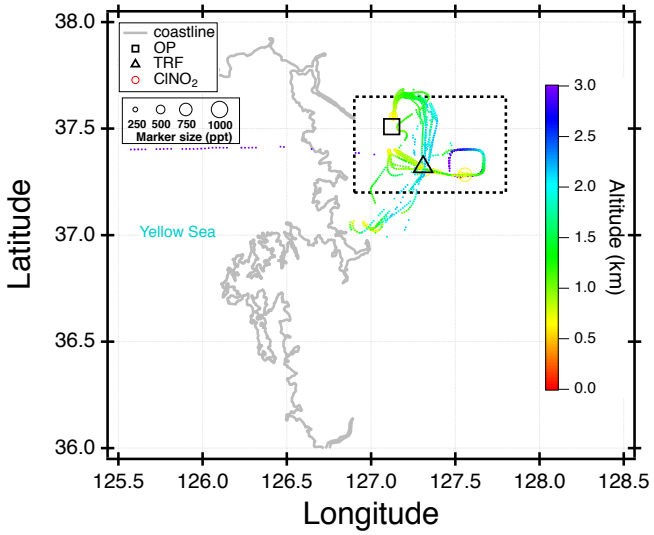

Figure S9. Airborne $ClNO_2$ data collected at 8:00 - 8:30 am local time during the whole campaign above 600 m. The black dashed box is the grid used for plotting vertical distribution of $ClNO_2$ in Figure 7. Markers size is proportional to the concentration of $ClNO_2$ and color coded with altitude.

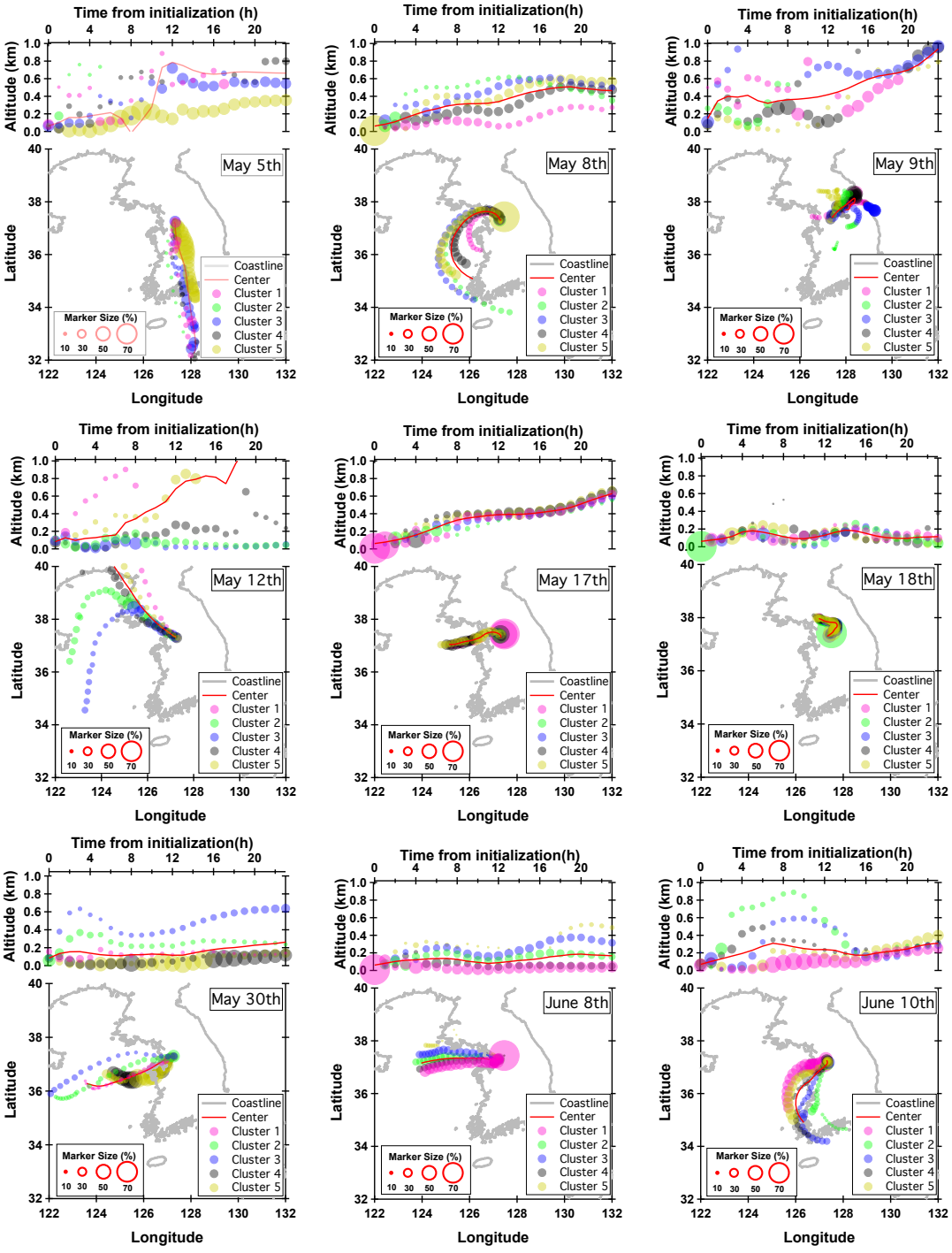

Figure S10. FLEXPART backtrajectories of the selected days when a second $ClNO_2$ peak was observed at TRF. Each run was initialized at 9:00 local time and each marker is an hour backward of its previous. The red line represents the center of the mass-weighted particles and the clusters are fractional contributions of airmasses in percentage.

References

Bertram, T. H. and Thornton, J. A.: Toward a general parameterization of N_2O_5 reactivity on aqueous particles: the competing effects of particle liquid water, nitrate and chloride, Atmos. Chem. Phy., 9, 8351–8363, https://doi.org/10.5194/acp-9-8351-2009, 2009.

Brown, S. S., Dubé, W. P., Tham, Y. J., Zha, Q., Xue, L., Poon, S., Wang, Z., Blake, D. R., Tsui, W., Parrish, D. D., and Wang, T.: Nighttime chemistry at a high altitude site above Hong Kong, J. Geophys. Res. Atmos., pp. 2457–2475, https://doi.org/10.1002/2015JD024566.Received, 2016.

Burkholder, J. B., Sander, S. P., Abbatt, J. P. D., Barker, J. R., Huie, R. E., Kolb, C. E., Kurylo, M. J., Orkin, V. L., Wilmouth, D. M., and Wine, P. H.: Chemical Kinetics and Photochemical Data for Use in Atmospheric Studies, Evaluation No. 18., Tech. rep., Jet Propulsion Laboratory, Pasadena, CA, 2015.

Clegg, S. L., Brimblecombe, P., and Wexler, A. S.: Thermodynamic Model of the System $H^+-NH_4^+-SO_4^{2-}-NO_3^--H_2O$ at Tropospheric Temperatures, J. Phys. Chem. A, 102, 2137–2154, https://doi.org/10.1021/jp973042r, http://pubs.acs.org/doi/abs/10.1021/jp973042r, 1998.

Crounse, J. D., McKinney, K. A., Kwan, A. J., and Wennberg, P. O.: Measurement of gas-phase hydroperoxides by chemical ionization mass spectrometry, Anal. Chem., 78, 6726–6732, https://doi.org/10.1021/ac0604235, 2006.

Deiber, G., George, C., Le Calvé, S., Schweitzer, F., and Mirabel, P.: Uptake study of $ClONO_2$ and $BrONO_2$ by Halide containing droplets, Atmos. Chem. Phy., 4, 1291–1299, https://doi.org/10.5194/acp-4-1291-2004, 2004.

Friese, E. and Ebel, A.: Temperature Dependent Thermodynamic Model of the System $H^+-NH_4^+-Na^+-SO_4^{2-}-NO_3^--Cl^--H_2O$, J. Phys. Chem. A, 114, 11 595–11 631, https://doi.org/10.1021/jp101041j, 2010.

Guo, H., Sullivan, A. P., Campuzano-Jost, P., Schroder, J. C., Lopez-Hilfiker, F. D., Dibb, J. E., Jimenez, J. L., Thornton, J. A., Brown, S. S., Nenes, A., and Weber, R. J.: Fine particle pH and the partitioning of nitric acid during winter in the northeastern United States, J. Geophys. Res., 121, 10 355–10 376, https://doi.org/10.1002/2016JD025311, 2016.

Guo, H., Liu, J., Froyd, K. D., Roberts, J. M., Veres, P. R., Hayes, P. L., Jimenez, J. L., Nenes, A., and Weber, R. J.: Fine particle pH and gas-particle phase partitioning of inorganic species in Pasadena, California, during the 2010 CalNex campaign, Atmos. Chem. Phy., 17, 5703–5719, https://doi.org/10.5194/acp-17-5703-2017, 2017.

Hanson, D. R. and Ravishankara, A. R.: Reactive Uptake of $ClONO_2$ onto Sulfuric Acid Due to Reaction with HCl and H_2O, J. Phy. Chem., 98, 5728–5735, https://doi.org/10.1021/j100073a026, 1994.

Hanson, D. R., Ravishankara, a. R., and Solomon, S.: Heterogeneous reactions in sulfuric acid aerosols: A framework for model calculations, J. Geophys. Res., 99, 3615, https://doi.org/10.1029/93JD02932, 1994.

Hennigan, C. J., Izumi, J., Sullivan, A. P., Weber, R. J., and Nenes, A.: A critical evaluation of proxy methods used to estimate the acidity of atmospheric particles, Atmos. Chem. Phy., 15, 2775–2790, https://doi.org/10.5194/acp-15-2775-2015, 2015.

Nault, B. A., Campuzano-Jost, P., Day, D. A., Schroder, J. C., Anderson, B., Beyersdorf, A. J., Blake, D. R., Brune, W. H., Choi, Y., Corr, C. A., de Gouw, J. A., Dibb, J., DiGangi, J. P., Diskin, G. S., Fried, A., Huey, L. G., Kim, M. J., Knote, C. J., Lamb, K. D., Lee, T., Park, T., Pusede, S. E., Scheuer, E., Thornhill, K. L., Woo, J. H., and Jimenez, J. L.: Secondary organic aerosol production from local emissions dominates the organic aerosol budget over Seoul, South Korea, during KORUS-AQ, Atmos. Chem. Phy., 18, 17 769–17 800, https://doi.org/10.5194/acp-18-17769-2018, 2018.

Song, S., Gao, M., Xu, W., Shao, J., Shi, G., Wang, S., Wang, Y., Sun, Y., and McElroy, M. B.: Fine-particle pH for Beijing winter haze as inferred from different thermodynamic equilibrium models, Atmos. Chem. Phy., 18, 7423–7438, https://doi.org/10.5194/acp-18-7423-2018, 2018.

Tham, Y. J., Wang, Z., Li, Q., Yun, H., Wang, W., Wang, X., Xue, L., Lu, K., Ma, N., Bohn, B., Li, X., Kecorius, S., Größ, J., Shao, M., Wiedensohler, A., Zhang, Y., and Wang, T.: Significant concentrations of nitryl chloride sustained in the morning: Investigations of the causes and impacts on ozone production in a polluted region of northern China, Atmos. Chem. Phy., 16, 14 959–14 977, https://doi.org/10.5194/acp-16-14959-2016, 2016.

Wang, H., Lu, K., Chen, X., Zhu, Q., Chen, Q., Guo, S., Jiang, M., Li, X., Shang, D., Tan, Z., Wu, Y., Wu, Z., Zou, Q., Zheng, Y., Zeng, L., Zhu, T., Hu, M., and Zhang, Y.: High N_2O_5Concentrations Observed in Urban Beijing: Implications of a Large Nitrate Formation Pathway, Environ. Sci. Technol. Lett., 10, 416–42, https://doi.org/10.1021/acs.estlett.7b00341, 2017a.

Wang, X., Wang, H., Xue, L., Wang, T., Wang, L., Gu, R., Wang, W., Tham, Y. J., Wang, Z., Yang, L., Chen, J., and Wang, W.: Observations of N_2O_5 and $ClNO_2$ at a polluted urban surface site in North China: High N_2O_5 uptake coefficients and low $ClNO_2$ product yields, Atmos. Environ., 156, 125–134, https://doi.org/10.1016/j.atmosenv.2017.02.035, 2017b.

Wang, Z., Wang, W., Tham, Y. J., Li, Q., Wang, H., Wen, L., Wang, X., and Wang, T.: Fast heterogeneous N_2O_5 uptake and $ClNO_2$ production in power plant and industrial plumes observed in the nocturnal residual layer over the North China Plain, Atmos. Chem. Phys, 175194, 12 361–12 378, https://doi.org/10.5194/acp-17-12361-2017, 2017c.

Wolfe, G. M., Marvin, M. R., Roberts, S. J., Travis, K. R., and Liao, J.: The framework for 0-D atmospheric modeling (F0AM) v3.1, Geosci. Model Dev., 9, 3309–3319, https://doi.org/10.5194/gmd-9-3309-2016, 2016.

Yun, H., Wang, W., Wang, T., Xia, M., Yu, C., Wang, Z., Poon, S. C. N., Yue, D., and Zhou, Y.: Nitrate formation from heterogeneous uptake of dinitrogen pentoxide during a severe winter haze in southern China, Atmos. Chem. Phys., 18, 17 515–17 527, https://doi.org/10.5194/acp-18-17515-2018, 2018.